East European Journal of Physics. 1. 217-232 (2025)
DOI: 10.26565/2312-4334-2025-1-23 ISSN 2312-4334

GRAPHENE OXIDE AND REDUCED GRAPHENE OXIDE AS HOLE TRANSPORT LAYERS FOR IMPROVED EFFICIENCY IN FULLERENE-BASED BULK HETEROJUNCTION ORGANIC SOLAR CELLS: A NUMERICAL SIMULATION STUDY

Denet Davis, K.S. Sudheer*
Optoelectronics Device Simulation Research Lab, Department of Physics, Christ College (Autonomous), Irinjalakuda, Thrissur, Kerala, India, 680125
University of Calicut, Calicut, Kerala, India, 673635
**Corresponding author: sudheersebastian@christcollegeijk.edu.in*
Received October 4, 2024; revised December 12, 2024; accepted January 13, 2025

A growing area of research in recent years has focused on improving the efficiency of [6,6]-phenyl-C61-butyric acid methyl ester (PCBM) fullerene-based bulk heterojunction organic solar cells (BHJOSC) using poly 3-hexylthiophene-2,5-diyl (P3HT) as the donor and graphene derivatives as the hole transport layer (HTL). Graphene derivatives, mainly graphene oxide (GO) and reduced graphene oxide (RGO), possess similar exceptional characteristics as that of graphene, and are good candidates as HTL in P3HT:PCBM based BHJOSC's. In this work, we use, One-Dimensional Solar Cell Capacitance Simulator (SCAPS1D) for the extensive and detailed study of two configurations, namely ITO/GO/P3HT:PCBM/Al and ITO/RGO/P3HT: PCBM/Al. Both configurations are optimized, and enhanced efficiencies are achieved by varying electrical input parameters of the device. Thereafter, design, simulation and analysis of different device combinations are done using nine distinct ETL's and three metal electrodes. ITO/GO/P3HT:PCBM/LiF/Ca and ITO/RGO/ P3HT:PCBM/LiF/Ca gave improved efficiencies of 8.00% and 12.00% respectively. Then, the influence of varying donor density of Lithium Fluoride (LiF), and effect of varying work function of Indium Tin oxide (ITO), on the device performance of these two devices is studied. A record efficiency of 16.47%, is attained for increased donor density of LiF in ITO/RGO/P3HT:PCBM/LiF/Ca configuration.
Keywords: *Bulk heterojunction organic solar cell; One Dimensional Solar Cell Capacitance Simulator; Graphene oxide; Reduced graphene oxide; Enhanced efficiency*
PACS: 85.60.-q, 84.60.Jt, 81.05.ue

1. INTRODUCTION

Bulk heterojunction (BHJ) organic photovoltaic (OPV) devices have garnered growing attention in research, driven by their promise for affordable, printable solar cells (SC) [1] that can be manufactured on flexible substrates. The typical composition of conventional BHJ photoactive material involves an interpenetrating network of electron-donor conjugated polymers [2] and electron-acceptor fullerenes, and among all the bulk heterojunction active materials, the mixture of solution-processed poly 3-hexylthiophene-2,5-diyl (P3HT) (as donor molecules) and fullerene derivative [6,6]-phenyl-C61-butyric acid methyl ester (PCBM) (as acceptor molecules) is the most researched blend [3–5]. In a simple BHJ device, both the donor and acceptor phases makes direct electrical contact with the cathode and anode, leading to recombination of carriers and current leakage [6-8]. Electron transport layers (ETL's) and hole transport layers (HTL's) are used to counteract these detrimental effects [7,8]. Identifying appropriate HTL and ETL with attention is critical for achieving improved stability and efficiency.

In the P3HT:PCBM based bulk heterojunction organic solar cell (BHJOSC), poly(3,4-ethylenedioxythiophene) polystyrene sulfonate (PEDOT:PSS) is the most extensively employed HTL [9-20]. This particular material is preferred because of its excellent conductivity and transparency, as well as its ability to improve the smoothness of the surface when applied on Indium Tin oxide (ITO). Nevertheless, the utilization of PEDOT: PSS comes with certain drawbacks, including its hygroscopicity, anisotropic charge injection, acidic nature, and batch-to-batch variations in electrical and physical properties. In order to investigate potential substitute materials for PEDOT:PSS in organic electronic devices, a great deal of research has been done [21]. In recent years graphene derivatives have emerged as a prominent alternative for PEDOT:PSS in P3HT:PCBM based bulk heterojunction organic solar cells (BHJOSC's).

Graphene oxide (GO) and reduced graphene oxide (RGO) are oxygen functionalized derivatives of graphene with a wider bandgap than graphene (0-4.66 eV) [22-27]. Since graphene is known to be the strongest and thinnest substance on Earth, with higher carrier mobility (1000–10000 $cm^2\ V^{-1}\ s^{-1}$), [28] zero bandgap, [29] and higher electrical conductivity, [30] breaking its chemical bonds is a highly challenging task. However, GO and RGO exhibit similar remarkable properties, which have the potential to enhance the stability of devices [31-32]. Moreover, GO/RGO shows promise as a superior substitute for PEDOT: PSS as the best HTL alternative. This is due to its adjustable electrical properties, work function compatibility with P3HT:PCBM, and potential for efficient and cost-effective manufacturing methods [33-36].

Since there are multiple affordable methods for fabricating GO and RGO from graphite and, graphite is more readily available than many other materials, we choose GO and RGO as HTL for our study. One state-of-the-art process for fabricating GO is the modified Hummer's method. GO is essentially graphene that contains functional groups with

Cite as: D. Davis, K.S. Sudheer, East Eur. J. Phys. 1, 217 (2025), https://doi.org/10.26565/2312-4334-2025-1-23

oxygen, including epoxides, hydroxyls, and carboxyl's. The modified Hummer's method entails the oxidation of graphite flakes using a combination of potent acids and oxidising agents [37-39]. GO is reduced to obtain RGO. The selection of the reduction technique relies on various factors, including safety concerns, the desired characteristics of the resulting RGO, and the intended purpose. After reduction, some of the oxygen functional groups are removed, and the resulting RGO exhibits improved electrical conductivity and other properties closer to pristine graphene [40-43].

GO possesses numerous oxygen functional groups, resulting in a broader bandgap compared to RGO. Consequently, the mobility of charge carriers becomes challenging. However, the reduction of GO to RGO diminishes the bandgap, rendering RGO more appropriate for electronic applications that require semi-conductive or conductive characteristics. RGO, with improved conductivity and reduced defects, will exhibit higher charge carrier mobility, which could contribute to efficient charge transport in bulk heterojunction organic solar cells [44-46].

Researchers have successfully fabricated BHJOSC with the configurations ITO/ GO/P3HT:PCBM/Al and ITO/RGO/P3HT:PCBM/Al in which ITO acts as the anode, and Aluminium (Al) acts as the cathode. In 2010, Shao *et al.* worked on ITO/GO/P3HT:PCBM/Al, with graphene oxide (made using the modified Hummer's method) as HTL with different thickness 2nm, 4nm, and 6 nm and attained 3.5%, 2%, and 0.9%, respectively [47]. The necessity of a simulation study on the effect of varying thicknesses of HTL and active layer exists. An extensive numerical simulation study on the effect on device performance with varying thickness of 5 nm to 100 nm has not been reported elsewhere, which we have carried out successfully and found the optimum thickness of HTL and active layer for better device performance.

In 2013, Jun *et al.* worked on P3HT:PCBM BHJOSC with similar configuration with graphene oxide nanoribbon as HTL. Notably, this solar cell device does not include an electron transport layer (ETL), and impressively, the fabricated device has an efficiency of approximately 4.02% [48]. For the past few years scientists and researchers have been introducing reduced graphene oxide as hole transport layer in BHJ OSC with P3HT:PCBM as active layer, ITO as anode, and Al as cathode with device configuration ITO/RGO/ P3HT:PCBM/Al. In 2011, Nguyen *et al.* reported 3.98% efficiency with RGO as HTL, [49] and later on, in the year 2020, Fakharan *et al.* reported an improved efficiency of 4.02% for RGO produced by Nd:YAG laser production as HTL for the same configuration [50]. Modelling and extended simulation study on ITO/GO/P3HT:PCBM/Al and ITO/RGO/ P3HT:PCBM/Al have not been reported elsewhere.

Our work includes extensive and detailed numerical simulation study, of configurations ITO/GO/P3HT:PCBM/Al, and ITO/RGO/P3HT:PCBM/Al, and improving their efficiency via optimisation. We have studied the influence of thickness, electron mobility, hole mobility, and defect density of active layer on the device performance. The effect of thickness, defect density, electron mobility, hole mobility and acceptor density of HTL, interface layer defect, series resistance, shunt resistance, and operating temperature is also studied. After optimisation of ITO/GO/P3HT:PCBM/Al, we achieved an efficiency of 4.32%, which is much greater than 1.63% (standardized work)[51] and optimisation of ITO/RGO/P3HT:PCBM/Al gave an enhanced efficiency of 6.65%, which is much higher than 0.65%(standardized work) [51]. In the intention of improving device performance, we design and simulate various device combinations, by incorporating nine diverse ETL's and three cathodes. The ETL's used include, N,N'- Bis(N,N-dimethylpropan-1-amine oxide)perylene-3,4,9,10-tetracarboxylic diimide (PDINO), Poly(9,9-bis(3'-(N,N-dimethyl) -N-ethylammoinium-propyl-2,7-fluorene)-alt-2,7-(9,9-dioctylfluorene)) dibromide (PFN-Br), Zinc oxide (ZnO), Lithium Fluoride (LiF), Indium gallium zinc oxide (IGZO), C60, [6,6]-phenyl-C_{61}-butyric acid methyl ester (PCBM) and Titanium dioxide: graphene composite (TiO_2:gr) and nitrogen doped graphene(n-graphene). Whereas, Aluminium (Al), Calcium (Ca) and Silver (Ag) are the three cathodes used for the study. Enhanced efficiencies of 8.00% and 12.00% is attained for the BHJOSC's with configuration ITO/GO /P3HT:PCBM/LiF/Ca and ITO/RGO/P3HT:PCBM/LiF/Ca respectively. Thereafter, the influence of varying donor density of LiF (ETL) on the device performance of configurations ITO/GO/P3HT:PCBM/LiF/Ca and ITO/RGO/P3HT:PCBM/LiF/Ca is also studied. A record high efficiency of 16.47%, Open circuit voltage (*Voc*) of 0.7389V, short circuit current density (*Jsc*) of 26.733287mA/cm^2 and fill factor (*FF*) of 83.36% is achieved for ITO/RGO/P3HT:PCBM/LiF/Al for increased donor density of LiF. The effect of varying work function of ITO on these configurations is also examined and no significant enhancement in efficiency is attained. From our studies, it can be concluded that RGO (bandgap-1.5 eV), when used as HTL, seems to produce a higher efficiency, when compared to GO (bandgap-2.48eV). Device with Ca (2.9eV), [52] placed as cathode seem to give better device performance compared to Al (4.2eV), [53] and Ag (4.35eV) [54].

2. METHODOLOGY, MODELLING AND PARAMETER SETTING

A One-Dimensional Solar Cell Capacitance Simulator (SCAPS1D) is used for the simulation. By solving the semiconductor equations, including Poisson's equation (Eq. 1), continuity equations for electrons (Eq. 2), and equations for holes (Eq. 3), which are provided below, the software creates a working point solution in steady state [55].

$$\frac{\partial}{\partial x}\left(\varepsilon_0 \varepsilon(x) \frac{\partial \Psi}{\partial x}\right) = -q\left[-n + p - N_A^- + N_D^+ \frac{\rho_{def}(n,p)}{q}\right] \quad (1)$$

$$-\frac{\partial J_n}{\partial x} - U_n(n,p) + G = \frac{\partial n}{\partial t} \quad (2)$$

$$\frac{-\partial J_p}{\partial x} - Up(n,p) + G = \frac{\partial p}{\partial t} \quad (3)$$

where ε is the dielectric permittivity, ε_0 is the permittivity of free space, Ψ *is* the electrostatic potential, n is the carrier concentration of electrons, p is the carrier concentration of holes, N_D^+ is the ionized donor concentration, N_A^+ is the ionized acceptor concentration, $\rho_{def}(n,p)$ is the distribution of defects, J_n is the electron current density, and J_p is the hole current density. U_n is the recombination rate of electrons, U_p is the recombination rate of holes, and G is the generation rate. The electron and hole current densities are given by the charge transport equations. D_n and D_p are electron and hole diffusion coefficients. Electron and hole mobilities are denoted by μ_n and μ_p respectively [55].

$$J_n = D_n \frac{dn}{dx} + \mu_n n \frac{d\phi}{dx} \tag{4}$$

$$J_p = D_p \frac{dn}{dx} + \mu_p p \frac{d\phi}{dx} \tag{5}$$

The schematic diagram of simulated device structure is shown in Fig. 1 (a), and Fig. 1 (b) gives the energy band diagram of layers used in the simulation study (GO, RGO, P3HT:PCBM, PDINO, PFN-Br, LiF, ZnO, IGZO, C60, PCBM, TiO_2:gr and n-graphene). The numerical input parameters of the active layer and the hole transport layers is listed in Table 1 and the input parameters of electron transport layers is listed in Table 2 and Table 3. The input parameters are taken from previous literature.

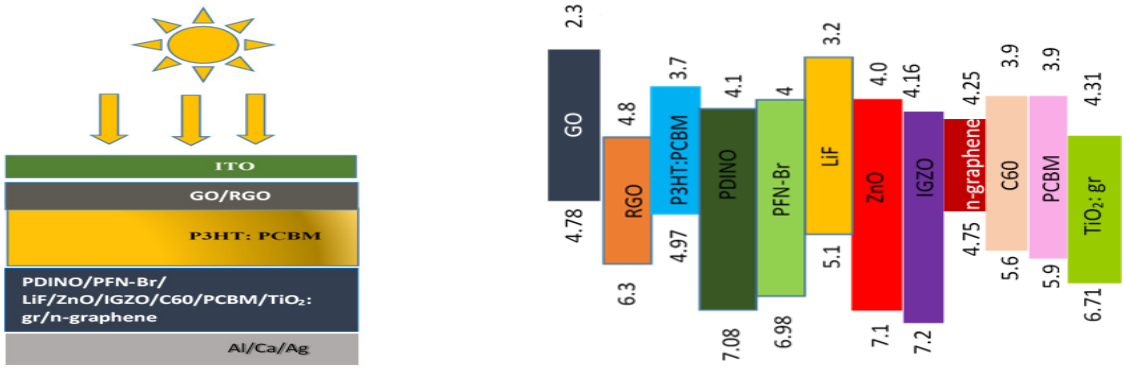

(a) **(b)**

Figure 1. Modelling of BHJOSC device: (a) schematic diagram of device structure, and (b) energy band diagram of layers GO, RGO, P3HT: PCBM, PDINO, PFN-Br, LiF, ZnO, IGZO, C60, PCBM, TiO_2:gr, and n-graphene

Capture cross section, electron and hole thermal velocity, for all layers are set to 1×10^{-15} cm^2, and 1×10^7cm/s, respectively. Furthermore, the capture cross-section for the HTL/active layer interface, and active layer/ETL interface is chosen as $1\times10^{-19}cm^2$. As in SCAPS1D, the energy level with respect to the reference (eV) is kept constant for all layers, at 0.6eV. The simulation is run at 323K operating temperature under AM1.5G light with an intensity of 1000mW/cm^2. The parameter values that are not mentioned in the table are set as given in SCAPS1D. The listed input parameters are used to standardize configurations ITO/GO/P3HT:PCBM/Al and ITO/RGO/P3HT:PCBM/Al.

Table 1. Numerical input parameters of active layer P3HT:PCBM and hole transport layer RGO

Parameters	P3HT:PCBM	Graphene oxide	Reduced graphene oxide
Thickness (nm)	100 [51]	35 [51]	35 [51]
Bandgap (E_g) (eV)	1.27 [56]	2.48 [59]	1.5 [60]
Electron affinity (χ) (eV)	3.7 [56]	2.3 [59]	4.8 [61]
Dielectric permittivity (ε_r)	3.5 [5]	10 [59]	13.3 [62]
Conduction band density CB (cm^{-3})	7.8×10^{19} [57]	1.8×10^{18} [59]	1×10^{19} [63]
Valence band density VB (cm^{-3})	7.8×10^{19} [57]	2.2×10^{18} [59]	1×10^{19} [63]
Thermal velocity of electrons V_e (cm/s)	1×10^7 [58]	1×10^7 [59]	1×10^7
Thermal velocity of holes V_h (cm/s)	1×10^7 [58]	1×10^7 [59]	1×10^7
Electron mobility μ_e (cm^2/Vs)	2×10^{-3} [58]	2.6×10^1 [59]	3.2×10^2 [64]
Hole mobility μ_h (cm^2/Vs)	2×10^{-3} [58]	1.23×10^2 [59]	3.2×10^2 [64]
Donor density N_D (cm^{-3})	0 [57]	0 [59]	0
Acceptor density N_A (cm^{-3})	0 [57]	1×10^{18} [59]	1×10^{18}
Defect density N_t (cm^{-3})	6.847×10^{15}	1×10^9 [59]	1×10^9

Table 2. Numerical input parameters of electron transport layers PDINO, PFN-Br, LiF, ZnO

Parameters	PDINO	PFN-Br	LiF	ZnO
Thickness (nm)	5 [65]	5 [66]	20 [67]	20 [71]
E_g (eV)	2.98 [65]	2.98 [66]	1.9 (varied) [68]	3.1 [72]
χ (eV)	4.1 [65]	4 [66]	3.2[68,69]	4 [73]

Parameters	PDINO	PFN-Br	LiF	ZnO
ε	5 [65]	5 [66]	9.1 [70]	9 [74]
CB (cm^{-3})	1×10^{19} [65]	1×10^{19} [66]	1×10^{20} [67,69]	2×10^{18} [74]
VB (cm^{-3})	1×10^{19} [65]	1×10^{18} [66]	1×10^{20} [67,69]	1.8×10^{19} [74]
V_e(cm/s)	1×10^{7} [65]	1×10^{7} [66]	1×10^{7} [69]	1×10^{7} [74]
V_h(cm/s)	1×10^{7} [65]	1×10^{7} [66]	1×10^{7} [69]	1×10^{7} [74]
μ_e (cm^2/Vs)	2×10^{-6} [65]	2×10^{-6} [66]	1 [67,69]	1×10^{2} [74]
μ_h (cm^2/Vs)	1×10^{-3} [65]	1×10^{-4} [66]	1 [67,69]	2.5×10^{2} [74]
N_D (cm^{-3})	2×10^{21} [65]	9×10^{18} [66]	1×10^{18} [67]	1×10^{18} [74]
N_A (cm^{-3})	0 [65]	0 [66]	0	0 [75]
N_t (cm^{-3})	1×10^{9}	1×10^{14} [66]	1×10^{9}	1×10^{14} [74]

Table 3. Numerical input parameters of electron transport layers IGZO, PCBM, C60, TiO_2: gr and n-graphene

Parameters	**IGZO** [75]	**PCBM** [75]	**C60** [75]	**TiO_2:graphene** [76]	**n-graphene** [77]
Thickness (nm)	5	5	5	50	0.334
E_g (eV)	3.05	2	1.7	2.4	0.5
(χ) (eV)	4.16	3.9	3.9	4.31	4.8
(ε)	10	3.9	4.2	7.8	10
CB (cm^{-3})	1×10^{19}	1×10^{19}	1×10^{19}	1×10^{19}	3×10^{19}
VB (cm^{-3})	1×10^{19}	1×10^{19}	1×10^{19}	1×10^{19}	3×10^{19}
V_e (cm/s)	1×10^{7}	1×10^{7}	1×10^{7}	1×10^{7}	1×10^{7}
V_h (cm/s)	1×10^{7}	1×10^{7}	1×10^{7}	1×10^{7}	1×10^{7}
μ_e (cm^2/Vs)	15	0.02	8×10^{-2}	350	10
μ_h (cm^2/Vs)	0.1	0.02	3.5×10^{-3}	350	1×10^{5}
N_D (cm^{-3})	1×10^{19}	1×10^{19}	1×10^{19}	5×10^{18}	1×10^{26}
N_A (cm^{-3})	0	0	0	0	0
N_t (cm^{-3})	1×10^{19}	1×10^{19}	1×10^{19}	1×10^{14}	1×10^{14}

3. STANDARDIZATION

A definite requirement for software validation is standardisation. The configurations, ITO/GO/P3HT:PCBM/Al and ITO/RGO/P3HT:PCBM/Al, are studied in our work, in which efficiencies of 1.63% and 0.65% are achieved [51]. Table 4 and Table 5 summarizes the validation of software via comparison of simulated and experimental outcome.

Table 4. Output parameters of ITO/GO/P3HT:PCBM/Al

	Voc (V)	*Jsc* (mA/cm^2)	*FF* (%)	Efficiency (%)
Experimental	0.57±0.02	6.94±0.1	41.2±0.01	1.63±0.01
Simulation	0.5329	7.6325	40.88	1.66

Table 5. Output parameters of ITO/RGO/P3HT: PCBM/Al

	Voc (V)	Jsc (mA/cm^2)	FF (%)	Efficiency (%)
Experimental	0.38±0.02	5.37±0.4	31.2±0.03	0.65±0.13
Simulation	0.3945	5.78	28.41	0.65

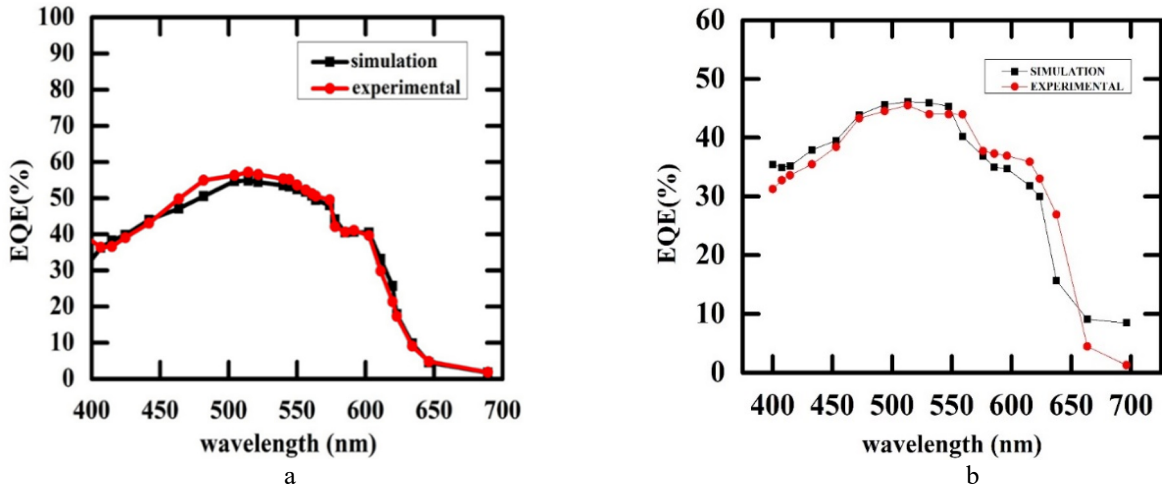

Figure 2. The matched experimental and simulation quantum efficiency graph of: (a) ITO/GO/P3HT:PCBM/Al, and (b) ITO/RGO/P3HT:PCBM/Al

Fig. 2 (a) and Fig. 2 (b) shows the matched quantum efficiency (*QE*) graph obtained from experimental results and simulation results of ITO/GO/P3HT:PCBM/Al and ITO/RGO/P3HT:PCBM/Al respectively.

4. RESULTS AND DISCUSSION

4.1. ITO/GO/P3HT: PCBM/Al

With the aim of designing a high efficiency BHJOSC with graphene oxide as HTL, an extensive numerical simulation study of ITO/GO/P3HT:PCBM/Al is done. The impact of electrical parameters, including thickness, defect density, electron mobility, and hole mobility of active layer, is studied. The effect of thickness, defect density, electron mobility, hole mobility, and acceptor density of HTL is also studied. In addition, the influence of interface (GO/P3HT:PCBM interface) defect, operating temperature, series resistance, and shunt resistance is also investigated. The device is optimised. Combination of device structures with nine distinct ETL's (PDINO, PFN-Br, LiF, ZnO, IGZO, C60, PCBM, TiO_2:gr, and n-graphene) and three metal contacts are simulated and analysed. The influence of donor density of ETL and effect of varying ITO work function on device performance of best configuration is also examined.

4.1.1. Influence of various electrical parameters of P3HT:PCBM

The input electrical parameters of the active layer play a crucial and significant role in improving the device stability and performance. The effect of input electrical parameters on device output parameters is studied and plotted in Fig. 3. The thickness of the active layer is a very important parameter for the smooth performance of BHJOSC. The thickness of the photoactive material is varied, from 20nm to 120nm, and the effect on output parameters is studied, and plotted in Fig. 3(a). As the thickness of the active material increases, efficiency rises, to a maximum value of 1.81% at 70nm and, then decreases. The reason for this is that once the thickness surpasses a specific limit (known as the optimum value), the charge carriers will need to cover a greater distance in order to reach the respective electrodes.

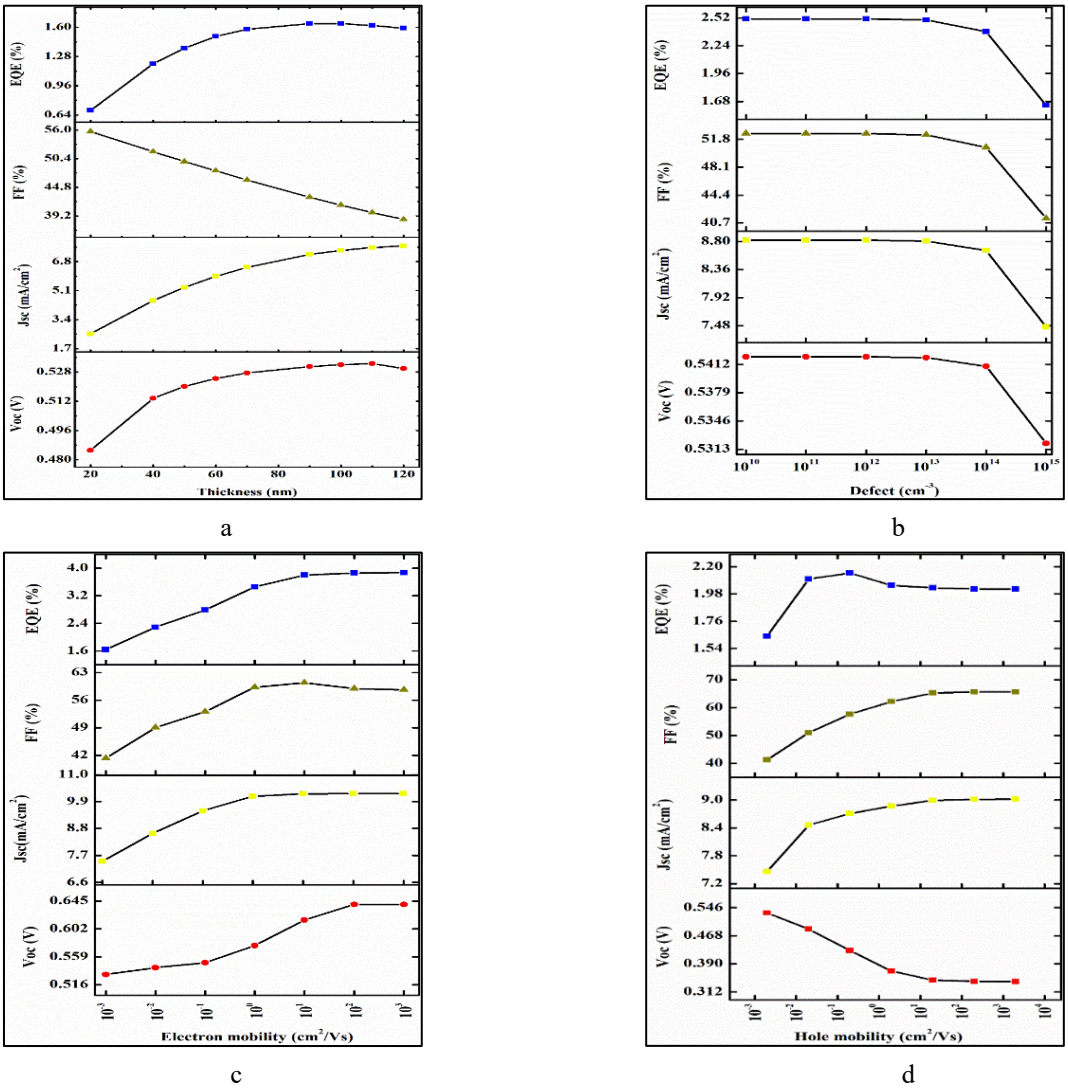

Figure 3. Variation of device output parameters of ITO/GO/P3HT:PCBM/Al with varying factors of active layer: (a) thickness, (b) defect density, (c) electron mobility, and (d) hole mobility

Consequently, as the thickness exceeds the optimum value, the efficiency declines. It is essential to increase the thickness up to a certain level to ensure optimal device performance, as this enhances light absorption and the generation of excitons.

Even though the device shows an improved efficiency at 70nm, when it comes to practical applications, 100nm is often considered as the optimum thickness for the active layer in P3HT:PCBM based BHJOSC's.

The impact of active layer defect density on device performance is depicted in Fig. 3(b). As the defect increases, from 10^{10} to 10^{15} cm^{-3}, efficiency decreases, from 2.45% to 1.66%. As defect density increases, the lifetime of carriers diminishes, resulting in an elevated recombination rate that impacts the performance of the device. A reduced defect density within the layer signifies a more polished surface, thereby contributing to a smoother device performance. Higher charge carrier mobility is necessary to reduce charge recombination as well as to promote charge collection. Fig. 3(c) and Fig. 3(d) show the effect of varying electron mobility and hole mobility of active layer on device performance. The electron mobility is varied from $2\times10^{-3}cm^2/Vs$ to $2\times10^{3}cm^2$ /Vs and a relatively enhanced efficiency of 4.11%, for $2\times10^{3}cm^2/Vs$ is attained. As the hole mobility increases, from $2\times10^{-3}cm^2/Vs$ to $2\times10^{3}cm^2/Vs$, efficiency reaches, a maximum value of 2.10% at $2\times10^{-1}cm^2/Vs$. The rise in material conductivity is affirmed by the increase in mobility. The balance of mobilities is predominantly upheld, as an imbalanced charge transport could potentially transpire if μ_e is lower.

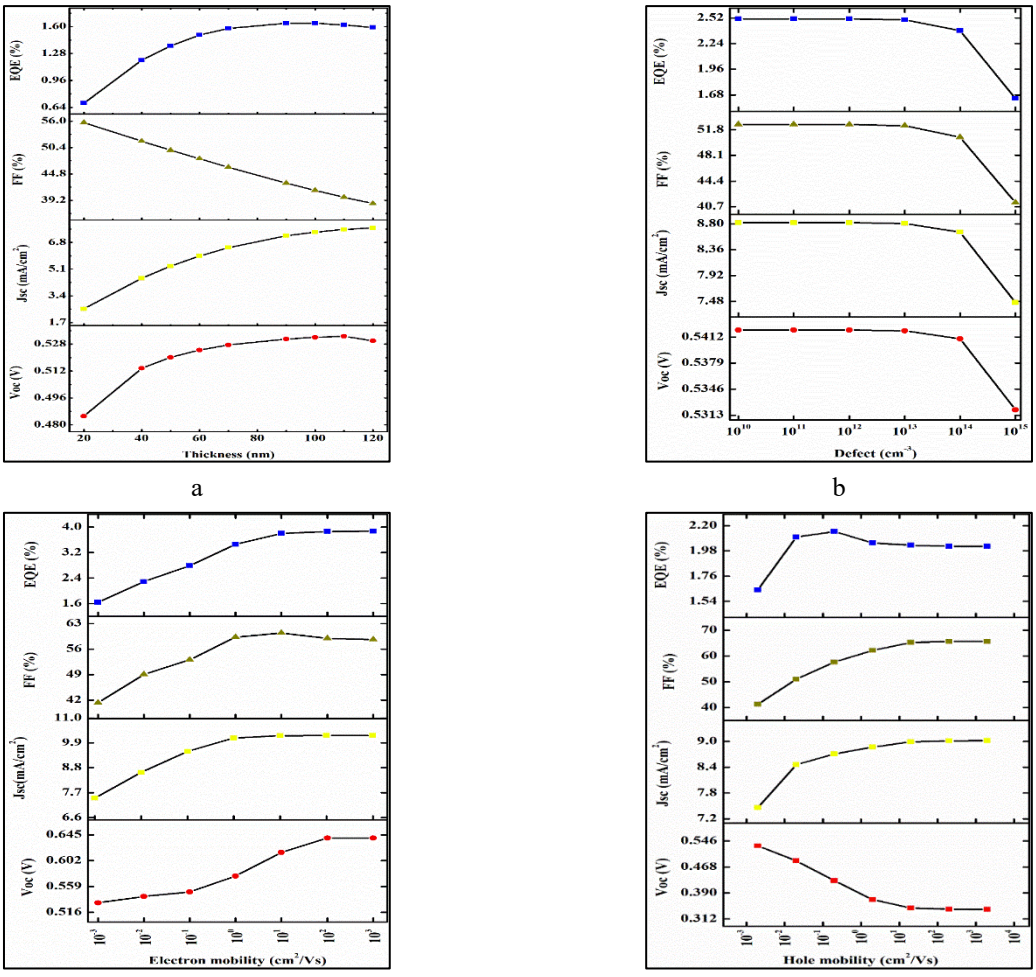

Figure 3. Variation of device output parameters of ITO/GO/P3HT:PCBM/Al with varying factors of active layer: (a) thickness, (b) defect density, (c) electron mobility, and (d) hole mobility

4.1.2. Influence of various electrical parameters of graphene oxide

The influence of the hole transport layer thickness on device performance is shown in Fig. 4(a). As the thickness for GO increases, efficiency reaches a maximum of 1.66% at 20nm, and then decreases. Researchers and device engineers often perform experiments and simulations to determine the ideal HTL thickness that maximises device efficiency. It's worth noting that the optimal thickness can vary depending on the specific materials used in the solar cell, the design of the device, and the intended application. Excessive HTL thickness can contribute to increased series resistance in the device, which can limit charge transport and reduce overall device performance. The experimental work chosen for standardisation has fabricated a BHJOSC device with 35nm thickness of GO. Our simulation study shows, 20nm thickness of GO gives good efficiency. This could be extremely helpful for the experimental fabrication of thin layered HTL in BHJOSC. Too thin or too thick HTL layers might be challenging to deposit reliably and uniformly during the manufacturing process.

As the defect of GO is varied, from 10^9 to 10^{15} cm^{-3} as shown in Fig. 4(b), efficiency remain unchanged. The device performance is not significantly affected by the defect density of graphene oxide, as indicated by this observation. However, it is preferable to have a minimal defect in the HTL layer in order to enhance its functionality.

The plot showing significance of electron and hole mobility of graphene oxide layer on device performance is given in Fig. 4(c) and Fig. 4(d). As the electron mobility of graphene oxide increases, efficiency gets improved and reaches 3.9%. The efficiency remains constant at as hole mobility changes from 2.6×10^{-3} to $2.6\times10^{3}cm^2/Vs$. The balance between electron and hole mobility is also maintained in the hole transport layer.

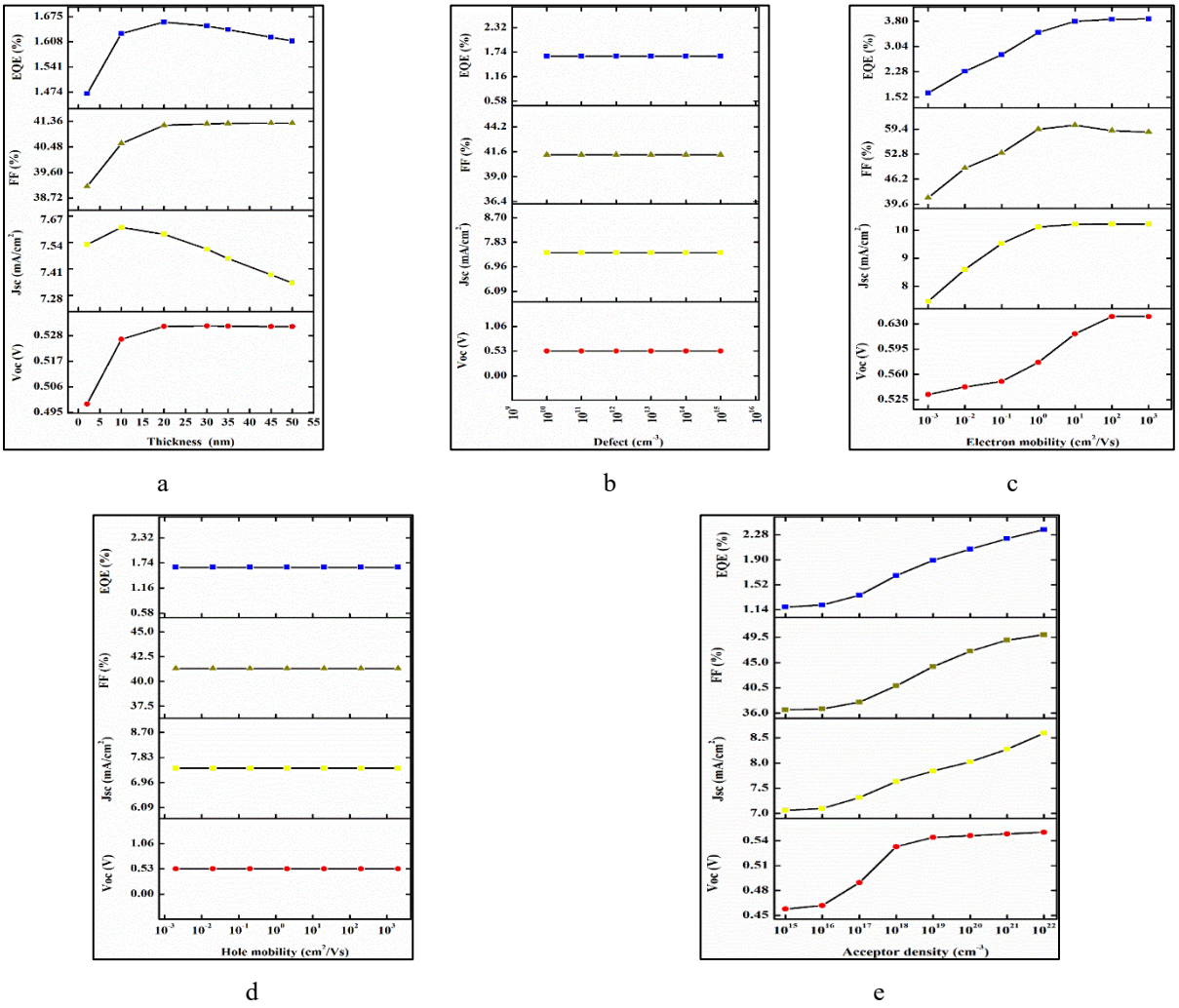

Figure 4. Variation of device output parameters of ITO/GO/P3HT:PCBM/Al with varying factors of HTL: (a) thickness, (b) defect density, (c) effect of electron mobility, (d) hole mobility, and (e) effect of acceptor density

The effect of varying acceptor density on device performance is also studied in this work. As the acceptor density is raised from $1\times10^{15}cm^{-3}$ to 1×10^{22} cm^{-3}, efficiency seems to increase and reaches 2.36%. Fig. 4(e) clearly shows the influence of varying acceptor density of GO on device performance. The acceptor density is varied from 1×10^{15} cm^{-3} to 1×10^{22} cm^{-3}. The efficiency seemed to increase with an increase in acceptor density. Maximum efficiency of 2.36% is achieved for 1×10^{22} cm^{-3}.

4.1.3. Influence of interface defect, temperature, series resistance and shunt resistance on the device performance

The interface defined in ITO/GO/P3HT:PCBM/Al is HTL/active layer interface (i.e grapheneoxide/P3HT:PCBM interface). Fig. 5(a) depicts the variation of device parameters with respect to change in interface defect values. The simulation is done by varying the density of interface ranging from 1×10^{10} cm^{-2} to 1×10^{15} cm^{-2}. Efficiency also decreases from 2.00% to 1.66% at 1×10^{14} cm^{-2}. It is evident from our research that achieving a low interface defect density is crucial for enhancing the performance of output devices. These findings align well with our previous results. Minimizing defects in the layers contributes to a smoother device performance. However, it is important to acknowledge that a certain level of defects is inevitable in materials and should be duly considered.

The operating temperature is varied from 250K to 500K and the device performance is studied as it appears in Fig. 5(b). The rise in temperature has a detrimental impact on the functionality of the device, resulting in a gradual decline in

performance. This decline can be attributed to the escalation in series resistance, which subsequently leads to an increase in recombination rate. It is worth noting that the influence of temperature is more pronounced in organic solar cells as opposed to inorganic solar cells. As the temperature increases from 250K to 500K, efficiency declines to 0.98%. Maintaining the device stability at very low temperature or very high temperature is a tedious task. The standardized devices are operated at a temperature of 323K, therefore, for optimization studies, the same operating temperature is utilized.

The variation of photovoltaic parameters with varying series resistance and shunt resistance is shown in Fig. 5(c) and Fig. 5(d) respectively. As the series resistance increases, from 1 to 10 Ω, efficiency decreases, from 1.59% to 1.52%. As the shunt resistance increases from 10 to 100000Ω, efficiency increases from 0.04% to 1.6%. An ideal device is commonly regarded as having no resistance. Resistances arise from leakage current, which is widely recognized as a significant concern in all device architectures.

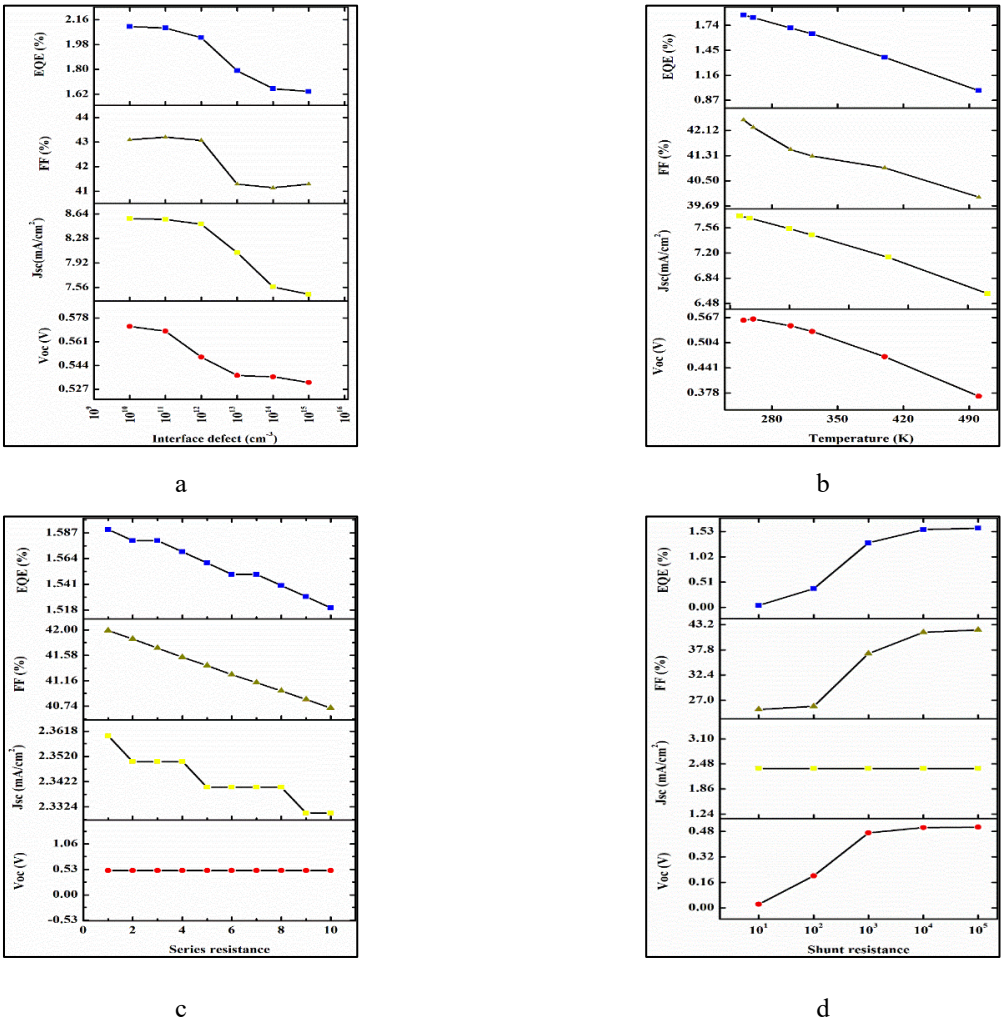

Figure 5. Variation of device output parameters of ITO/GO/P3HT:PCBM/Al with varying factors: (a) interface defect, (b) temperature, (c) series resistance, and (d) shunt resistance

After the extended numerical simulation study we optimized device configuration ITO/GO/P3HT:PCBM/Al. Table 6 summarizes the optimized output parameters after simulation. The optimized input parameters for active layer and HTL corresponds to thickness of 70nm and 20nm respectively, defect density of 6.847×10^{10} and 1.9×10^{10} cm^{-3} electron mobility of 2×10^{-3} and $2.6\times10^{3}cm^2/Vs$, hole mobility of 2×10^{-1} and $1.23\times10^{3}cm^2/Vs$.

Table 6. Optimized output values of ITO/GO/P3HT:PCBM/Al

Voc (V)	Jsc (mA/cm^2)	FF (%)	EQE (%)
0.6237	8.92765	77.6	4.32

4.1.4. Influence of diverse ETL's and different metal electrodes on device performance

The electron transport layer is crucial in boosting the efficiency of BHJOSC. The inclusion of ETL's will indeed enhance the device's performance by optimizing the transportation of charge carriers. Followed by optimisation, designing and simulation study of various combination are done with three metal electrodes (Al, Ca and Ag) and diverse ETL's (PDINO, PFN-Br, LiF, ZnO, IGZO, PCBM, C60, TiO_2:gr and n-graphene). Table 7 lists the *Voc*, *Jsc*, *FF*, and Efficiency

attained for various device configurations. Improved *Voc* of 0.9277V is attained for ITO/GO/P3HT:PCBM/PFN-Br/Al. The device ITO/GO/P3HT: PCBM/LiF/Ca gives maximum *Jsc* of 11.498525mA/cm^2 and high efficiency of 8.00%. Highest fill factor of 84.29% is achieved for the device ITO/GO/P3HT:PCBM/IGZO/Ca.

The comparison shows that device combinations with Ca as cathode showed better device performance. Our simulation study clearly shows enhanced efficiency (greater than 6.00%) for most of the configurations.

Table 7. Device output parameters of ITO/GO/P3HT: PCBM/ETL/cathode with diverse ETL's and cathodes

Back metal contact	ETL	*Voc* (V)	*Jsc* (mA/cm^2)	*FF* (%)	Efficiency (%)
Aluminium	PDINO	0.9255	10.816248	76.29	7.63
	PFN-Br	0.9277	11.4186	58.02	6.15
	LiF	0.4298	10.31244	76.88	6.01
	ZnO	0.9088	10.413318	77.43	7.33
	IGZO	0.7161	10.442410	83.63	6.25
	PCBM	0.8196	10.555798	76.74	6.64
	C60	0.8207	10.651364	76.62	6.70
	TiO_2:graphene	0.6104	10.434697	81.73	5.21
	n-graphene	0.3679	10.428822	74.44	2.86
Calcium	PDINO	0.9523	10.2493	75.85	7.40
	PFN-Br	0.8490	11.2198	81.73	7.79
	LiF	0.8517	11.498525	81.73	8.00
	ZnO	0.9186	8.868	77.58	6.32
	IGZO	0.7456	10.435529	84.29	6.56
	PCBM	0.9213	10.565869	76.55	7.45
	C60	0.9229	10.663121	76.44	7.52
	TiO_2:graphene	0.6104	10.434699	81.73	5.21
	n-graphene	0.3679	10.428695	74.44	2.86
Silver	PDINO	0.8908	9.68514	72.34	6.24
	PFN-Br	0.5766	10.05635	63.83	3.70
	LiF	0.2919	10.19363	67.48	2.01
	ZnO	0.8497	9.69244	79.38	6.54
	IGZO	0.5961	10.438554	81.26	5.06
	PCBM	0.8303	10.428956	64.99	5.65
	C60	0.8463	10.535471	73.20	6.53
	TiO_2:graphene	0.6104	10.434179	81.73	5.21
	n-graphene	0.3667	10.428614	74.41	2.85

4.1.5. Influence of donor density of ETL on the device performance of ITO/GO/P3HT:PCBM/LiF/Ca

The influence of donor density of Lithium Flouride (ETL) on the device performance of ITO/GO/P3HT:PCBM/LiF/Al is studied and plotted in Fig. 6. As the donor density is raised from 1×10^{15} to 1×10^{22}cm^{-3}, the efficiency first improves to 8.15% at 1×10^{19} cm^{-3}, remains a constant and then decreases.

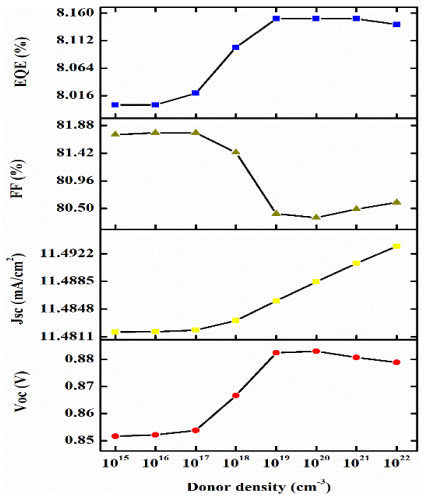

Figure 6. Influence of donor density of LiF (ETL) on device performance of ITO/RGO/P3HT:PCBM/LiF/Al

4.1.6 Influence of varying ITO work function

The impact of different work functions of ITO (anode) on the performance of, device with maximum efficiency (ITO/GO/P3HT:PCBM/LiF/Ca) is also investigated. We vary the ITO work function within the range of 4.7 to 5.00eV, and analyse the device's performance. However, only a small increase in efficiency is seen in the device's performance. Only a marginal improvement of 0.1% in efficiency is achieved when the work function is increased to 5.00eV.

4.2. ITO/RGO/P3HT: PCBM/Al

An extensive numerical simulation study of ITO/RGO/P3HT:PCBM/Al is done. The effect of thickness, defect density, electron mobility, and hole mobility of active layer, is studied. The influence of varying input parameters such as thickness, defect density, electron mobility, hole mobility, and acceptor density of HTL is also studied. Furthermore, the examination extends to the influence of interface defects (RGO/P3HT:PCBM interface), operating temperature, series resistance, and shunt resistance.

The device is optimised, and then various combination of device structures is studied. Nine ETL's (PDINO, PFN-Br, LiF, ZnO, IGZO, C60, PCBM, TiO_2:gr, and n-graphene) and three metal contacts are used to design various combinations. Study on influence of donor density of LiF (ETL) is carried out and effect of varying ITO work functions on device performance is also studied.

4.2.1. The effect of varying electrical properties of active layer on device performance

The impact of varying the active layer's thickness and defect density on the *Voc*, *Jsc*, *FF*, and efficiency is investigated and considered for device optimization. We have varied the thickness of active layer in the range of 5 to 200 nm, and the associated effect on device outcomes is analysed by maintaining all other factors constant throughout the simulations.

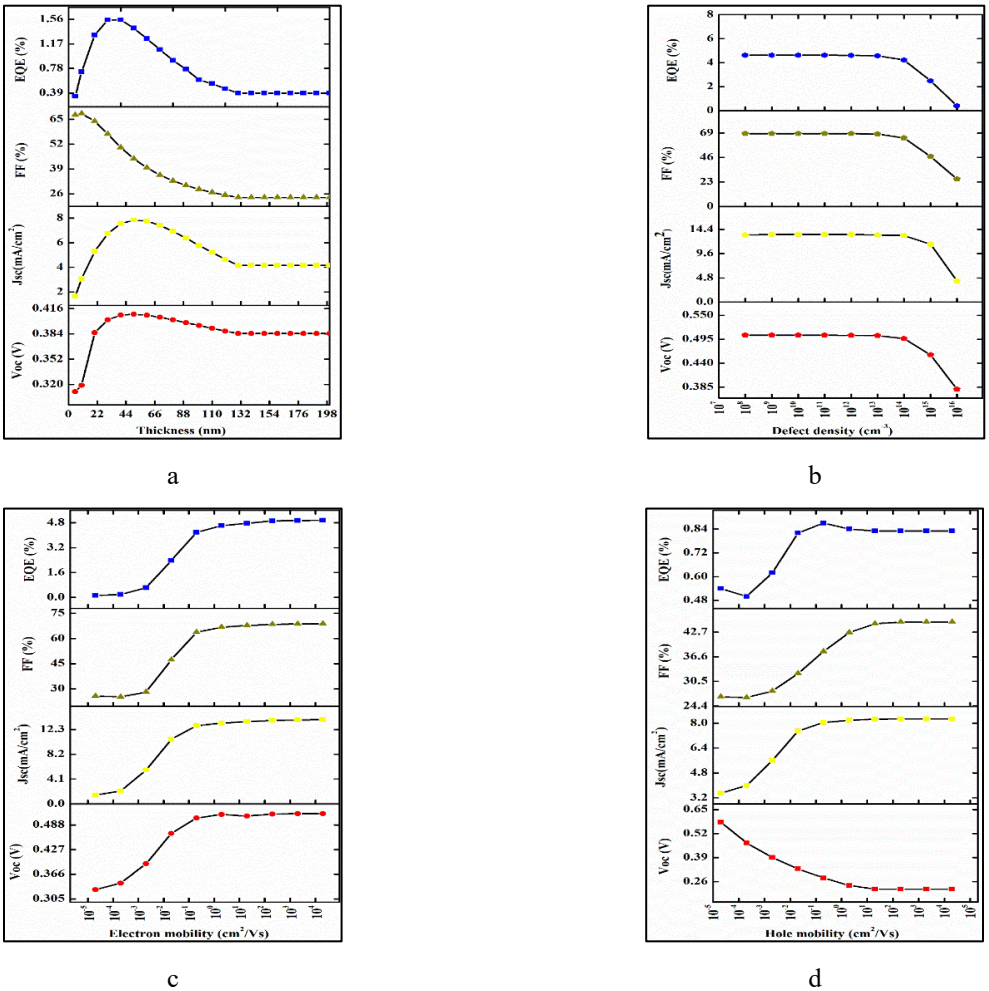

Figure 7. Variation of device output parameters of ITO/RGO/P3HT:PCBM/Al with varying factors of active layer: (a) thickness, (b) defect density, (c) electron mobility and (d) hole mobility, (a) thickness (b) defect density (c) effect of electron mobility and (d) effect of hole mobility

The effect of varying active layer thickness on device performance is shown in Fig. 7 (a), and a maximum efficiency of 1.55% is attained at 50nm. Even though we got 50nm as the optimum thickness, for P3HT:PCBM based BHJOSC 100nm is applied in experimental works.

As the thickness increases, there is a clear rise in the surface area of the active layer. Increasing the thickness up to a certain point is crucial for achieving optimal device performance, as it enhances the absorption of photons and the generation of electron-hole pairs. However, once the thickness exceeds the ideal value, the efficiency begins to decline. This can be attributed to the fact that, beyond a certain thickness limit (the optimum value), the charge carriers have to travel a greater distance to reach the corresponding electrodes.

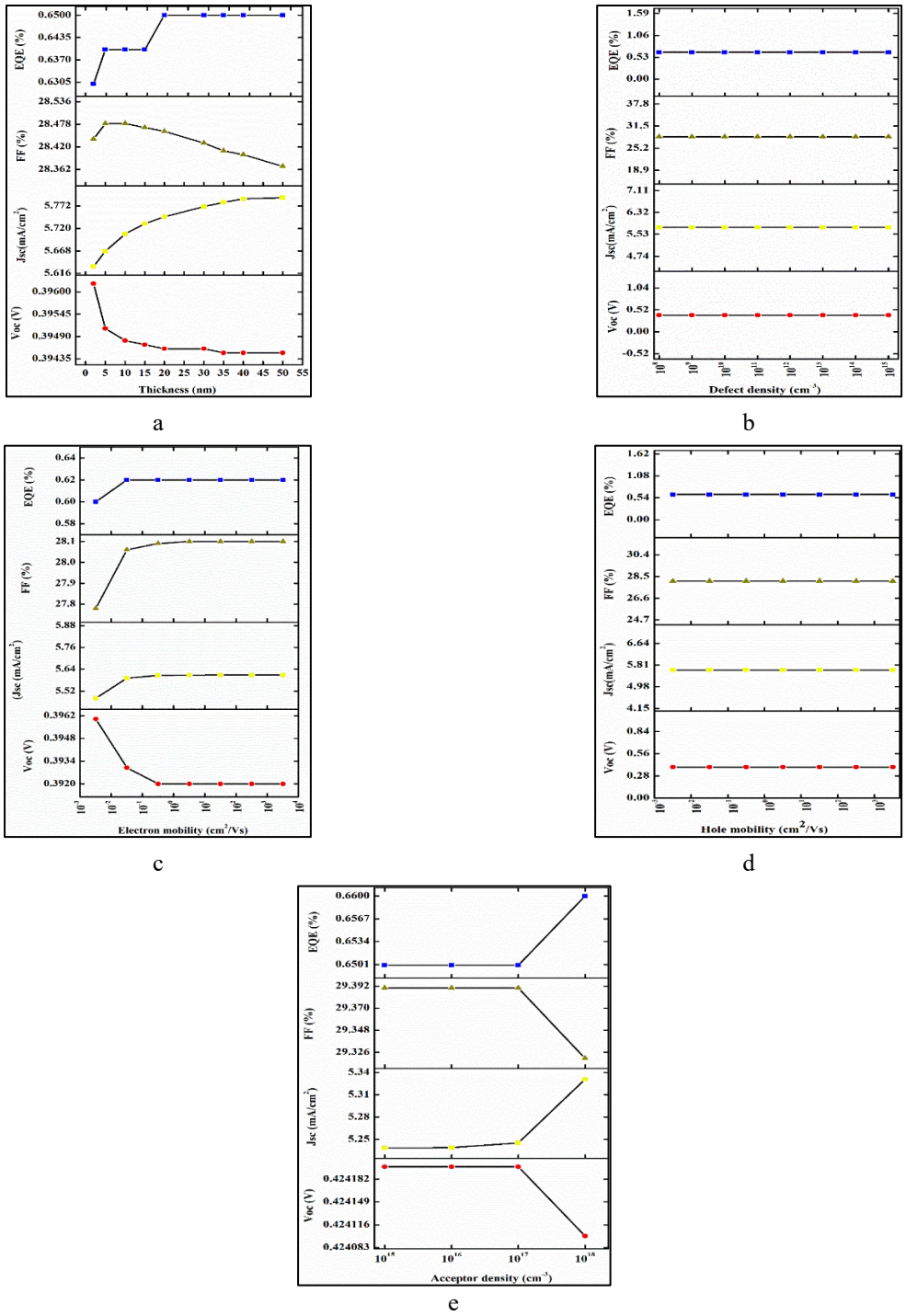

Figure 8. Variation of device output parameters of ITO/RGO/P3HT:PCBM/Al with varying factors of HTL: (a) thickness, (b) defect density, (c) electron mobility (d) hole mobility, and (e) acceptor density

Consequently, an increase in thickness beyond the optimum value significantly increases the likelihood of charge carrier recombination. Ultimately, this results in a decrease in the device's output parameters after reaching the optimum thickness value.

As the defect increases from 10^8 to 10^{16} cm^{-3}, efficiency decreases to 0.41% as shown in Fig. 7(b). The performance of the device is greatly influenced by the defect density present in the active layer. Achieving a defect-free active layer via fabrication is an extremely difficult task and is practically unattainable. Simulation study with excessive defect density in active layer is also avoided in the study, as it could significantly damage the device and impact its performance.

As the electron mobility is increased to $2\times10^4 cm^2/Vs$, efficiency increases upto 4.95%. Fig. 7(c) shows the effect of variation of electron mobility of active layer on device performance. Higher charge mobility is necessary to reduce the charge recombination as well as promote the charge collection. The effect of variation of hole mobilitiy of active layer on device performance is shown in Fig. 7(d).

As the hole mobility of the active layer is increased, efficiency of 0.86% is attained for $2\times10^4 cm^2/Vs$. The equilibrium of mobility is upheld, as the movement of electrons through the layers becomes more challenging when, μ_e is lower. An unbalanced charge transport might possibly occur if mobility range is unbalanced. The possibility of an imbalanced charge transport arises when there is an uneven distribution in the range of mobility.

4.2.2 The effect of variation of electrical properties of HTL on device performance

The effect of varying input parameters of HTL on the device performance is shown in Fig. 8. As shown in Fig. 8(a), efficiency reaches a maximum of 0.65% at 20nm thickness of RGO and then decreases. If the HTL is too thin, it might lead to incomplete hole collection, resulting in lower current and reduced efficiency. Conversely, excessive thickness of the HTL may hinder charge transport, leading to similar performance problems. The thickness of the HTL can impact the ease of hole movement within the layer and their ability to reach the anode.

As the defect of the RGO is increased from 10^8 to 10^{16} cm^{-3}, the device output parameters remain constant as shown in Fig. 8(b). This study shows that varying defect density of RGO (HTL), has no significant impact on the device performance.

The effect of varying electron and hole mobilities of RGO on device performance, is shown in Fig. 8(c) and Fig. 8(d). At an electron mobility of $3.2\times10^1 cm^2/Vs$, efficiency reaches 0.62%. As the hole mobility of RGO increases, the device performance remains unaffected.

Influence of acceptor density of HTL is shown in Fig. 8(e). As the acceptor density is raised, from 1×10^{15} to 1×10^{18} cm^{-3}, initially the efficiency remains constant at 0.65% and then improves to 0.66%.

4.2.3 Effect of interface defect, operating temperature, series resistance and shunt resistance.

The effect of interface defect on device performance is shown in Fig. 9(a). As the interface defect is increased from $10^{14}1/cm^2$ to $10^{20}1/cm^2$, an increase in efficiency of 0.62% at $1\times10^{17}1/cm^2$. The interface is the reason for separation of charge carrier and reach electrodes. Introduction of HTL actually improves this, and due to the HTL/active layer interface, charge separation will occur more.

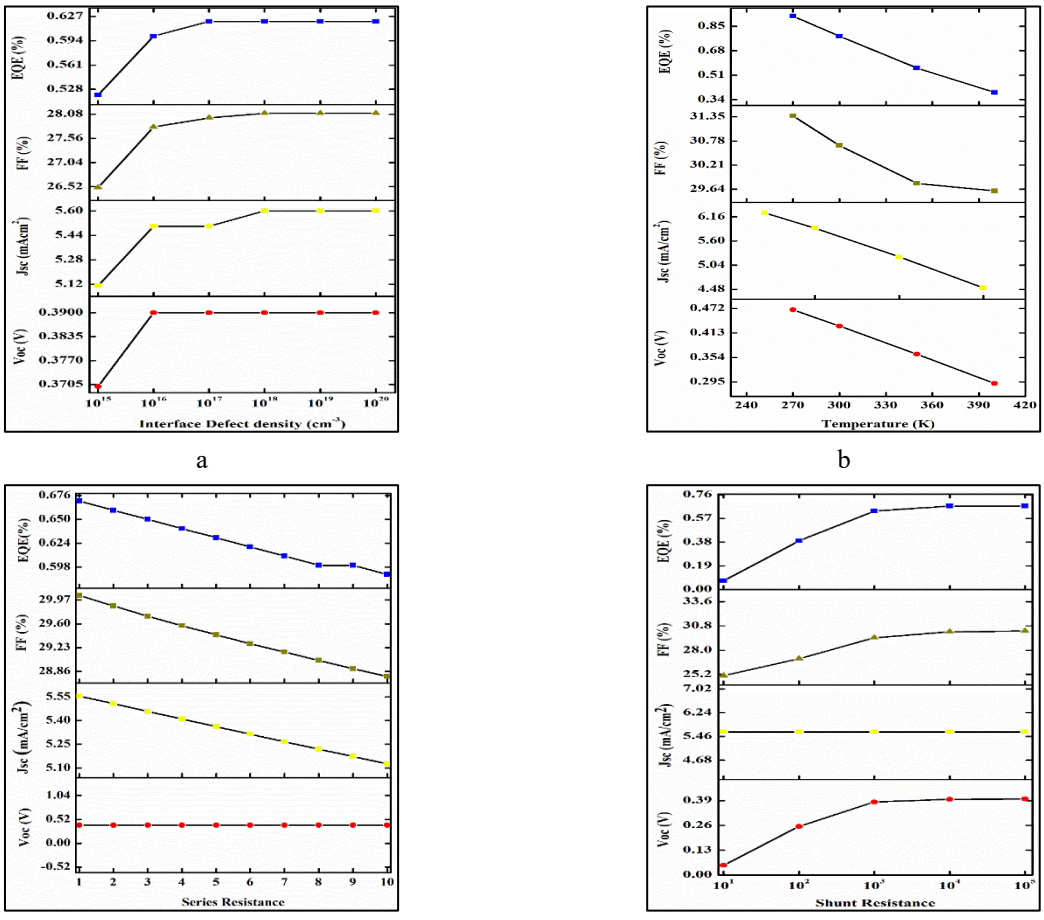

Figure 9. Variation of device output parameters of ITO/RGO/P3HT:PCBM/Al with varying factors: (a) interface defect, (b) temperature, (c) series resistance, and (d) shunt resistance

While it is generally preferred to minimize defects in the device for optimal performance, a certain level of interface defect is necessary. Neglecting the presence of this specific range of interface defect would be impractical in real-world applications.

As the temperature increases, the device output parameters are seen to be affected badly as shown in Fig. 9(b). As it reaches 600 K, efficiency reaches 0.03%. A gradual decrease in efficiency is seen. As the temperature rises, the series resistance also increases, resulting in a higher recombination rate. Organic solar cells are more significantly affected by temperature compared to inorganic solar cells. In order to conduct optimization studies, the operating temperature is established at 323K.

Fig. 9(c) and Fig. 9(d) represents the variation of photovoltaic parameters with varying series resistance and shunt resistance respectively. As the series resistance increases from 1 to 10 ohm, efficiency decreases from 0.67% to 0.59%. At open-circuit voltage, series resistance has no effect on the solar cell because there is no total current flow across the series resistance and the solar cell itself. As the shunt resistance increases from 10 to 100000 Ω, efficiency increases from 0.07% to 0.67%. The shunt resistance has no effect on the short circuit current, while the efficiency seems to increase. An ideal device is commonly regarded as having zero resistance, although the existence of such devices remains unknown. Conversely, the majority of fabricated devices possess a minimum level of resistance.

The optimization of the ITO/RGO/P3HT:PCBM/Al device has been conducted, taking into account all the aforementioned findings. The optimized thickness for active layer and HTL corresponds to 100nm and 35 nm respectively. Defect density of 5.39×10^{12} and 1.9×10^{19} cm^{-3} is chosen for active layer and HTL respectively. Electron mobility and hole mobility of active layer and HTL are chosen as 2×10^{4} and $2\times10^{-1}cm^2/Vs$, and 3.2×10^{1} and $3.2\times10^{4}cm^2/Vs$ correspondingly.

ITO/RGO/P3HT:PCBM/Al is optimized and the optimized output values are as shown in Table 8. After optimization, the efficiency of the device is significantly increased by 6.65%, surpassing the efficiency of the standardized device (0.65%).

Table 8. Device output parameters of ITO/RGO/P3HT:PCBM/Al after optimization.

Voc (V)	Jsc (mA/cm^2)	FF (%)	Efficiency (%)
0.7130	11.704530	79.73	6.65

4.2.4 ITO/RGO/P3HT:PCBM/Al with diverse electron transport layers and different cathodes

We were able to attain an efficiency of 6.65% after optimising ITO/RGO/P3HT:PCBM/ Al. Different combinations of devices are designed, simulated and analysed for improved device performance using nine ETL's and three cathodes. Introducing ETL's can actually enhance device performance via enhanced charge carrier transmission. The improvement in efficiency and device output performance with the implementation of electron transport layers is carried out. The ETL's used for this study includes PDINO, PFN-Br, ZnO, IGZO, C60, PCBM, TiO_2: gr and n-graphene. We also explore the impact of distinct cathodes, with varying work functions such as Al, Ca, and Ag. As we introduce the ETL's and cathodes band alignment of the layers is essential for the proper working of device. This is achieved by appropriately varying the electron affinity values of different layers.

Among the different configurations studied, device with configuration ITO/RGO/ P3HT:PCBM/LiF/Ca, gave a record high efficiency of 12.00%, high *Voc* of 0.7909 V and enhanced *Jsc* of $26.613796mA/cm^2$. High *FF* of 81.12% was attained for the configuration ITO/RGO/P3HT:PCBM/C60/Ca. RGO has a lower bandgap compared to GO, making RGO more similar to graphene. The band alignment of RGO is also in well agreement with that of P3HT:PCBM. The electronic and optical properties of RGO is more tunable. RGO can also be doped according to the necessity of the device. Experimental studies on P3HT:PCBM based BHJOSC with RGO as HTL exists in literature, yet an extensive simulation study with diverse ETL's and different cathodes is not reported elsewhere. Table 9 lists the device output parameters of ITO/RGO/P3HT:PCBM/ETL/Cathode. Cathode has the lowest work function compared to Aluminium (4.2eV) and silver (4.35eV).

Table 9. The device output parameters of various combinations simulated using ITO/RGO/P3HT:PCBM/ETL/Cathode.

Back metal contact	**ETL**	***Voc* (V)**	***Jsc* (mA/cm^2)**	***FF* (%)**	**Efficiency (%)**
Aluminium	PDINO	0.7309	11.84	81.07	7.02
	PFN-Br	0.7271	12.04	71.39	6.25
	LiF	0.577	12.49604	68.92	4.97
	ZnO	0.7309	11.83136	81.08	7.01
	IGZO	0.7309	11.77	81.08	6.97
	PCBM	0.731	11.74159	76.73	6.59
	C60	0.731	11.76	79.69	6.85
	TiO_2:graphene	0.7311	11.75	80.71	6.93
	n-graphene	0.5189	11.493991	70.54	4.21
Calcium	PDINO	0.731	11.8781	81.1	7.04
	PFN-Br	0.7324	12.2746	79.21	7.12
	LiF	0.7909	26.613796	56.99	12.00
	ZnO	0.731	11.87096	81.1	7.04

Back metal contact	ETL	*Voc* (V)	*Jsc* (mA/cm^2)	*FF* (%)	Efficiency (%)
	IGZO	0.7309	11.77554	81.11	6.98
	PCBM	0.7309	11.77595	81.11	6.98
	C60	0.7309	11.77854	81.12	6.98
	TiO_2:graphene	0.7311	11.74356	80.71	6.93
	n-graphene	0.5207	11.494086	70.46	4.22
Silver	PDINO	0.7308	11.81524	76.87	6.64
	PFN-Br	0.6252	11.98285	61.65	4.62
	LiF	0.4271	12.28191	64.77	3.4
	ZnO	0.7308	11.77807	81.06	6.98
	IGZO	0.7312	11.73301	80.51	6.91
	PCBM	0.7307	11.69365	59.69	5.1
	C60	0.7631	11.8055	59.89	5.4
	TiO_2:graphene	0.7311	11.74356	80.71	6.93
	n-graphene	0.4506	11.493799	72.44	3.75

4.2.5 Influence of donor density of ETL on the device performance of ITO/RGO/P3HT:PCBM/LiF/Ca

The influence of donor density of Lithium Flouride (ETL) on the device performance of ITO/RGO/P3HT:PCBM/LiF/Al is studied and plotted in Fig. 10. As the donor density is raised from 1×10^{15} to 1×10^{22}cm^{-3}, the efficiency first improved to 16.47% at 1×10^{20} cm^{-3} and subsequently showed a slight decrease.

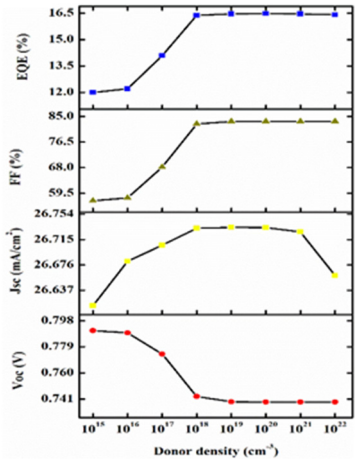

Figure 10. Influence of donor density of LiF (ETL) on device performance of ITO/RGO/P3HT:PCBM/LiF/Al

4.2.6 Influence of varying ITO work function

The impact of different work functions of ITO (anode) on the performance of, device with maximum efficiency (ITO/RGO/P3HT:PCBM/LiF/Ca) is also investigated. We vary the ITO work function within the range of 4.7 to 5.00eV, and analyse the device's performance. Nevertheless, there is no notable enhancement observed in the device's performance. Only a slight improvement of 0.09% in efficiency is attained when the work function is raised to 5.0eV.

5. CONCLUSIONS

The design and simulation of BHJOSC with the configurations ITO/GO/P3HT:PCBM/Al and ITO/RGO/P3HT:PCBM/Al have been successfully carried out in this study. The influence of input parameters of active layer and HTL, on the device performance is analysed. In addition, the influence of interface defects, series resistance, shunt resistance, and temperature is also examined.

Both the devices are optimised and an improved efficiency of 4.32% is obtained for ITO/GO/P3HT:PCBM/Al, and an increased efficiency of 6.65% is attained for ITO/RGO/P3HT:PCBM/Al. Followed by optimisation, designing and simulation study of various combinations of devices is studied using nine different ETL's and three metal contacts with different work function, (Al, Ca and Ag). The device configuration ITO/GO/ P3HT:PCBM/LiF/Ca achieved an enhanced efficiency of 8.00%. The device configuration ITO/RGO/P3HT:PCBM/LiF/Ca, exhibited a record efficiency of 12.00%. Thereafter, the influence of donor density of ETL (LiF) is also examined, and it is seen that, efficiency can be improved by increasing the donor density of ETL. The impact of changing the ITO work function on the device performance of configurations ITO/GO/P3HT:PCBM/Al and ITO/RGO/P3HT:PCBM/Ca was then investigated, which only resulted in, 0.1% and 0.09% improvement in the device efficiency respectively.

The findings of our research suggest that RGO is a more favorable choice as a hole transport layer (HTL) compared to GO. Additionally, LiF is identified as the best electron transport layer (ETL) for P3HT:PCBM based BHJOSC. Our

simulation studies have shown that Ca outperforms other cathodes in terms of achieving a high *Jsc*, increased *FF*, and enhanced efficiency. This can be attributed to the low work function property of Ca, indicating that BHJOSC performs exceptionally well with cathodes that have low work function.

Acknowledgment

The authors extend their heartfelt gratitude to Prof. Marc Burgelman from the University of Gent, Belgium for providing access to the SCAPS 1-D software.

Conflicts of interest

The authors declare that they have no relevant financial interests in the article and no other potential conflicts of interest to disclose.

ORCID

Denet Davis, https://orcid.org/0000-0001-6673-2499; **K.S. Sudheer**, https://orcid.org/0000-0002-9019-4405

REFERENCES

[1] H. Kang, et al., Adv. Mater. **28**, 7821 (2016). https://doi.org/10.1002/adma.201601197
[2] G. Yu, J. Gao, J.C. Hummelen, F. Wudl, and A.J. Heeger, Science, **270**, 1789 (1995). https://doi.org/10.1126/science.270.5243.1789
[3] T. Fukuda, *et al*., Phys. Status Solidi - Rapid Res. Lett. **5**, 229 (2011). https://doi.org/10.1002/pssr.201105232
[4] L. Lu, *et al*., Chem. Rev. **115**, 12666 (2015). https://doi.org/10.1021/acs.chemrev.5b00098
[5] B. Kadem, A. Hassan, and W.J. Cranton, J. Mater. Sci. Mater. Electron. **27**, 7038 (2016). https://doi.org/10.1007/s10854-016-4661-8
[6] S. Bichave, *et al*., Materials Today: Proceedings, (2023). https://doi.org/10.1016/j.matpr.2023.01.190
[7] H. Xu, *et al*., J. Mater. Chem. A, **8**, 11478 (2020). https://doi.org/10.1039/D0TA03511D
[8] S. Park, *et al*., Adv. Mater. **32**, 1 (2020).
[9] A.M. Mir, F. Bashir, F.A. Khanday, F. Zahoor, M. Hanif, and Z. May, IEEE Access, **12**, 10961 (2024). https://doi.org/10.1109/ACCESS.2024.3354163
[10] I. Masood, M.P. Singh, and M. Amir, "Analysis of Different Layers Thicknesses on the Performance of Organic Solar Cells," in: *2023 International Conference on Power, Instrumentation, Energy and Control* (*PIECON*), (Aligarh, 2023). pp. 1-5.
[11] M. Palewicz, A. Sikora, T. Piasecki, E. Gacka, P. Nitschke, P. Gnida, B. Jarząbek, and T. Gotszalk, Energies, **16**, 4741 (2023). https://doi.org/10.3390/en16124741
[12] D. Davis, M.S. Shamna, K.S. Nithya, and K.S. Sudheer, "Graphene as a hole transport layer for enhanced performance of P3HT:PCBM bulk heterojunction organic solar cell: a numerical simulation study," in: *IOP Conference Series: Materials Science and Engineering,* vol. 1248, (Jalandhar, Punjab, 2022), pp. 012011.
[13] G.R. Nishad, R.B. Younus, and P. Singh, "Applications of PEDOT: PSS in Solar Cells," in: *Materials for Solar Cell Technologies, II* **103**, 40 (2021), pp 40-76. https://doi.org/10.21741/9781644901410-3
[14] K.S. Ram, *et al*., Nanomater. **11**, 209 (2021). https://doi.org/10.3390/nano11010209
[15] J. Healey, *Conductive polymer films as electrodes in organic solar cells*, (Memorial University of Newfoundland, 2020).
[16] D. Ompong, *Designing thin film solar cells for optimum photovoltaic performance*, (Charles Darwin University, Australia, 2017).
[17] F. Hakim, and M.K. Alam, "Improvement of photo-current density of P3HT: PCBM bulk heterojunction organic solar cell using periodic nanostructures," in: *2017 International Conference on Electrical, Computer and Communication Engineering* (*ECCE*), (IEEE, 2017), pp. 170-174.
[18] F. Hakim, and Md.K. Alam, Sol. Energy, **191**, 300 (2019). https://doi.org/10.1016/j.solener.2019.08.073
[19] H.M. Rad, F. Zhu, and J. Singh, J. Appl. Phys. **124**, 083103 (2018). https://doi.org/10.1063/1.5031062
[20] Q. Zheng, *et al*., Sol. energy mater. sol. cells, **95**, 2200 (2011). https://doi.org/10.1016/j.solmat.2011.03.024
[21] J. Cameron, and P.J. Skabara, Mater. Horiz. **7**, 1759 (2020). https://doi.org/10.1039/C9MH01978B
[22] M.A. Velasco-Soto, *et al*., Carbon, **93**, 967 (2015). https://doi.org/10.1016/j.carbon.2015.06.013
[23] A. Iwan, and A. Chuchmała, Prog. Polym. Sci. **37**, 1805 (2012). https://doi.org/10.1016/j.progpolymsci.2012.08.001
[24] Y. Zhu, *et al*., Adv. Mater. **22**, 3906 (2010). https://doi.org/10.1002/adma.201001068
[25] R. Tarcan, *et al*., J. Mater. Chem. C, **8**, 1198 (2020). https://doi.org/10.1039/C9TC04916A
[26] N.O. Weiss, *et al*., Adv. Mater. **24**, 5782 (2012). https://doi.org/10.1002/adma.201201482
[27] K.I. Bolotin, *et al*., Solid State Commun. **146**, 351 (2008). https://doi.org/10.1016/j.ssc.2008.02.024
[28] K.I. Bolotin, "Electronic transport in graphene: Towards high mobility," in: *Graphene*, (Woodhead Publishing, 2014), pp. 199-227.
[29] X. Xu, *et al*., Chem. Soc. Rev. **47**, 3059 (2018). https://doi.org/10.1039/C7CS00836H
[30] M. Raji, N. Zari, Q.A. El Kacem, and R. Bouhfid, *Functionalized graphene nanocomposites and their derivatives*, (Elsevier, 2019).
[31] E. Singh, and H.S. Nalwa, RSC Adv. **5**, 73575 (2015). https://doi.org/10.1039/C5RA11771B
[32] B.V.R.S. Subramanyam, *et al*., J. Renew. Sustain. Energy, **12**, 054701 (2020). https://doi.org/10.1063/5.0021208
[33] J. Liu, *et al*., Adv. Mater. **26**, 786 (2014). https://dx.doi.org/10.1002/adma.201302987
[34] N.T. Ho, *et al*., Phys. Status Solidi Appl. Mater. Sci. **211**, 1873 (2014). https://doi.org/10.1002/pssa.201330611
[35] A. Van Dijken, *et al*., Organic Electronics, **4**, 131 (2003). https://doi.org/10.1016/j.orgel.2003.08.007
[36] J.M. Yun, *et al*., Adv. Mater. **23**, 4923 (2011). https://doi.org/10.1002/adma.201102207
[37] Y. Gao, *et al*., Appl. Phys. Lett. **97**, 203306 (2010). https://doi.org/10.1063/1.3507388
[38] A. Ali, *et al*., Curr. Appl. Phys. **18**, 599 (2018). https://doi.org/10.1016/j.cap.2018.02.016
[39] T.A. Amollo, G.T. Mola, and V.O. Nyamori, Sol. Energy, **171**, 83 (2018): https://doi.org/10.1016/j.solener.2018.06.068
[40] H.P. Kim, A.R.M. Yusoff, and J. Jang, Sol. Energy Mater. Sol. Cells, **110**, 87 (2013).
[41] N.M.S. Hidayah, *et al*., AIP Conf. Proc. **1892**, 150002 (2017). https://doi.org/10.1063/1.5005764
[42] Y.-J. Jeon, *et al*., Sol. Energy Mater. Sol. Cells, **105**, 96 (2012). https://doi.org/10.1016/j.solmat.2012.05.024
[43] A. Negash, A.M. Demeku, and L.H. Molloro, New J. Chem. **46**, 13001 (2022). https://doi.org/10.1039/D2NJ01974D
[44] Xu Xiang, *et al*., Carbon Letters, **32**, 557 (2022). https://doi.org/10.1007/s42823-021-00287-6

[45] T. Tene, *et al*., Front. Chem. **11**, (2023). https://doi.org/10.3389/fchem.2023.1267199
[46] Y. Wang, *et al*., Mater. Today, **21**, 186 (2018). https://doi.org/10.1016/j.mattod.2017.10.008
[47] S.S. Li, K.H. Tu, C.C. Lin, C.W. Chen, and M. Chhowalla, ACS Nano, **4,** 3169 (2010). https://doi.org/10.1021/nn100551j
[48] J. Liu, *et al*., Adv. Mater. **26**, 786 (2014). https://doi.org/10.1002/adma.201302987
[49] D.D. Nguyen, *et al*., Nanotechnology, **22**, 295606 (2011). https://doi.org/10.1088/0957-4484/22/29/295606
[50] Z. Fakharan, L. Naji, and K. Madanipour, Org. Electron. **76**, 105459 (2020). https://doi.org/10.1016/j.orgel.2019.105459
[51] J.H. Lee, *et al*., Org. Electron. **30**, 302 (2016). https://doi.org/10.1016/j.orgel.2016.01.003
[52] H. Park, P.R. Brown, V. Bulović, and J. Kong, Nano Lett. **12**, 133 (2012). https://doi.org/10.1021/nl2029859
[53] G.A. Chamberlain, Sol. Cells, **8,** 47 (1983). https://doi.org/10.1016/0379-6787(83)90039-X
[54] M. Akbi, "A method for measuring the photoelectric work function of contact materials versus temperature," in: *IEEE Transactions on Components, Packaging and Manufacturing Technology*, **4**(8), (2014), pp. 1293-1302. https://doi.org/10.1109/TCPMT.2014.2328661
[55] M. Burgelman, K. Decock, A. Niemegeers, J. Verschraegen, and S. Degrave, *SCAPS manual*, (University of Gent, 2023).
[56] S.B. Hacène, T. Benouaz, and T. Benouaz, Phys. Status Solidi (a), **211**, 862 (2014). https://doi.org/10.1002/pssa.201330320
[57] B.M. Omer, "Influence of characteristic energy of the valence band tail on performance of P3HT:PCBM bulk-heterojunction solar cell: AMPS-1D simulation study," in: *2014 IEEE 40th Photovoltaic Specialist Conference* (*PVSC)*, (IEEE, 2014), pp. 1770-1775.
[58] E.K. Chiew, M. Yahaya, and A. P. Othman, International Journal of Computational Materials Science and Engineering, **01**(01), 1250004 (2012). https://doi.org/10.1142/S2047684112500042
[59] G.A. Nowsherwan, *et al*., Nanomater. **12**, 1767 (2022). https://doi.org/10.3390/nano12101767
[60] A.S. Khune, *et al*., J. Electron. Mater. **52**, 8108 (2023). https://doi.org/10.1007/s11664-023-10711-4
[61] L. Sygellou, *et al*., J. Phys. Chem. C, **120**, 281 (2016). https://doi.org/10.1021/acs.jpcc.5b09234
[62] C. Yuwen, *et al*., Mater. Res. Express, **6**, 0950b4 (2019). https://doi.org/10.1088/2053-1591/ab149f
[63] A. Daraie, and A. Fattah, Opt. Mater. **109**, 110254 (2020). https://doi.org/10.1016/j.optmat.2020.110254
[64] W. Abdelaziz, *et al*., Sol. Energy, **211**, 375 (2020). https://doi.org/10.1016/j.solener.2020.09.068
[65] W. Abdelaziz, *et al*., Opt. Mater. **91**, 239 (2019). https://doi.org/10.1016/j.optmat.2019.03.023
[66] M.Q. Khokhar, *et al*., Mater. Sci. Semicond. Process. **134**, 105982 (2021). https://doi.org/10.1016/j.mssp.2021.105982
[67] S.-F. Wang, *et al*., J. Phys. Chem. C, **116**, 1650 (2012). https://doi.org/10.1021/jp2045146
[68] M.Q. Khokhar, *et al*., Energies, **13**, 1635 (2020). https://doi.org/10.3390/en13071635
[69] Jacob, Mohan V. Science and Technology of Advanced Materials **6** (2005): 944-949.
[70] H. Niu, *et al*., Dalton Transactions, **50**, 6477 (2021). https://doi.org/10.1039/D1DT00344E
[71] V. Srikant, and D.R. Clarke, J. Appl. Phys. **83**, 5447 (1998). https://doi.org/10.1063/1.367375
[72] B. Hussain, *et al*., Electronics, **8**(2), 238 (2019). https://doi.org/10.3390/electronics8020238
[73] A. Umar, *et al*., Micromachines, **13**(12), 2073 (2022). https://doi.org/10.3390/mi13122073
[74] K.S. Nithya, and K.S. Sudheer, Opt. Mater. **123**, 111912 (2022). https://doi.org/10.1016/j.optmat.2021.111912
[75] M. Dadashbeik, D. Fathi, and M. Eskandari, Sol. Energy, **207**, 917 (2020). https://doi.org/10.1016/j.solener.2020.06.102
[76] M.M. Shabat, G. Zoppi, "Simulation on the perovskite-based solar cell with graphene derivative," in: *The 8th International Engineering Conference on Renewable Energy & Sustainability*, (Gaza, Palestine, 2023).

ОКСИД ГРАФЕНУ ТА ВІДНОВЛЕНИЙ ОКСИД ГРАФЕНУ ЯК ДІРКОВІ ТРАНСПОРТНІ ШАРИ ДЛЯ ПІДВИЩЕННЯ ЕФЕКТИВНОСТІ ОБ'ЄМНИХ ГЕТЕРОПЕРЕХОДНИХ ОРГАНІЧНИХ СОНЯЧНИХ ЕЛЕМЕНТІВ НА ОСНОВІ ФУЛЕРЕНУ: ДОСЛІДЖЕННЯ ЧИСЛОВОГО МОДЕЛЮВАННЯ

Денет Девіс, К.С. Судхір

Дослідницька лабораторія моделювання оптоелектронних пристроїв, кафедра фізики, автономний Християнський коледж Іринджалакуда, Тріссур, Керала, Індія, 680125

Калікутський університет, Калікут, Керала, Індія, 673635

Останніми роками все більше досліджень зосереджено на покращенні ефективності об'ємних гетероперехідних органічних сонячних елементів (BHJOSC) на основі фулерену на основі метилового ефіру [6,6]-феніл-C61-масляної кислоти (PCBM) з використанням полі 3-гексилтіофен-2 ,5-діїл (P3HT) як донор і похідні графену як шар транспортування дірок (HTL). Похідні графену, головним чином оксид графену (GO) і відновлений оксид графену (RGO), мають такі ж виняткові характеристики, як і графен, і є хорошими кандидатами в якості HTL у BHJOSC на основі P3HT:PCBM. У цій роботі ми використовуємо симулятор одновимірної ємності сонячних елементів (SCAPS1D) для широкого та детального вивчення двох конфігурацій, а саме ITO/GO/P3HT:PCBM/Al та ITO/RGO/P3HT: PCBM/Al. Обидві конфігурації оптимізовані, а підвищена ефективність досягається зміною вхідних електричних параметрів пристрою. Після цього проектування, моделювання та аналіз різних комбінацій пристроїв виконуються з використанням дев'яти різних ETL і трьох металевих електродів. ITO/GO/P3HT:PCBM/LiF/Ca та ITO/RGO/P3HT:PCBM/LiF/Ca забезпечили підвищення ефективності на 8,00% і 12,00% відповідно. Потім вивчається вплив різної щільності донора фториду літію (LiF) і ефект змінної роботи виходу оксиду індію та олова (ITO) на продуктивність цих двох пристроїв. Рекордна ефективність 16,47% досягнута для підвищеної щільності донора LiF у конфігурації ITO/RGO/P3HT:PCBM/LiF/Ca.

Ключові слова: *об'ємний гетероперехідний органічний сонячний елемент; симулятор ємності одновимірної сонячної батареї; оксид графену; відновлений оксид графену; підвищена ефективність*